Conductance of perovskite oxide thin films and interfaces

Mubeen Dildar, I.

3

Sample fabrication and characterization

In the previous chapter, we have discussed the fundamental physics and the phase diagram of manganites, their sensitivity to the amount of doping, choice of substrate and micro structuring. Also, the interfaces between $LaAlO_3$ and $SrTiO_3$ were described as interesting candidates to study the physical properties of interfaces and reasons for the conduction at the interfaces. Such studies demand a high quality growth of the materials. After growth, the films should be characterized to confirm their crystalline quality, morphology and most important for $LaAlO_3$ and $SrTiO_3$, the interfaces. In this chapter, we give details of the deposition, information on targets and substrates, techniques used to characterize thin films.

Section 3.1 describes the sputter process and geometry, and discusses targets and substrates. Section 3.2 describes the characterization of the films by AFM (surface) and X-ray diffraction (bulk structure). Optical and electron beam lithographic techniques are described in section 3.4. The transport properties of films were measured by a physical properties measuring system (PPMS). Magnetic properties of films were measured by a SQUID-based magnetic properties measuring system (MPMS), described briefly in section 3.5. In the last section of the chapter, 3.6, we discuss the degradation of LCMO targets and a remedy to prolong its life time.

3.1 Sputtering

We used DC and RF sputtering techniques to grow the films which are studied in this thesis. Here we briefly describe them, including a discussion on the targets and substrates which were used.

3.1.1 DC and RF reactive sputtering

In reactive DC and RF sputtering of oxide materials, oxygen as a molecular gas incorporates in the growth process and compensates the deficiency of oxygen in the growing films. In normal DC sputtering, a dc power is applied between the cathode (target material) and anode (substrate) to ionize the argon gas. The newly formed Ar^+ ions accelerate towards the negatively charged cathode and a process of cascade ionization enables to sputter the target material. Ionization of molecular gases yields a negative valency which can cause backsputtering of the substrate. This can be avoided by choosing a high process pressure. The long path lengths of the ions to the substrate facilitates scattering and thermalization, and allow for on-axis sputtering. Off-axis sputtering can be used for the reactive gases even at low growth pressures [1].

Depending on the target material either DC or RF sputtering may be used. For a conducting target material, a constant voltage is used to accelerate the ions to the desired velocity. As the ions strike the surface, the resulting charges can move freely about the material to prevent any charge buildup. However, if the material is an insulator, as the ions strike the surface, their charge will remain localized and over time the charge will build up, making it impossible to further bombard the surface. In order to prevent this, alternating current is used at a frequency above 50 kHz. A high frequency is used so that the heavy ions cannot follow the switching fast enough and only electrons hit the surface to neutralize charge.

We used reactive DC sputtering to grow $La_{0.7}Sr_{0.3}MnO_3$ and $La_{0.7}Ca_{0.3}MnO_3$ thin films at high oxygen pressure of 3 mbar and 2.2 mbar. RF reactive sputtering was used to grow insulating $LaAlO_3$ films at 0.8 mbar (optimized pressure). Oxygen is used as reactive gas for both DC and RF sputtering.

3.1.2 Targets, substrates and thin film growth process

Targets

Conducting targets with nominal composition of $La_{0.7}Sr_{0.3}MnO_3$ (LSMO), $La_{0.7}Ca_{0.3}MnO_3$ (LCMO) and non-conducting $LaAlO_3$ (LAO) targets were purchased from commercial companies with a purity of 99.9% and density better than 96%. All materials, LSMO (the bulk lattice constant a_c is 3.863 Å), LCMO (a_c = 3.873 Å) and LAO (a_c = 3.79 Å) belong to the family of perovskites. For the growth of LAO films, we used stoichiometric and non-stoichiometric targets to try to vary the amount of aluminum in the respective films. The stoichiometric target is $La_1Al_1O_3$ and the non-stoichiometric target is $La_{0.94}Al_{1.06}O_3$. For the best epitaxial match with the films, perovskites substrates are used. The almost inevitable mismatch between film and substrate leads to strain as given in Table 3.1.

Substrates

$SrTiO_3$ (STO hereafter) (001) is a standard perovskite substrates used for the growth of manganites. The high dielectric constant of STO make them very use-

ful for gating experiments. The mismatch between LSMO, LCMO and LAO films with STO substrate gives tensile strain. The commercially available STO substrates have surfaces with equal amounts of SrO (AO) and TiO_2 (BO_2) - terminated domains separated by half unit-cell steps. Figure 3.1a shows as received STO which has mixed termination of both SrO and TiO_2 top layers. A line-profile of an untreated substrate (Figure 3.1b) gives a variation of about 0.2 nm. Such mixed terminated STO substrates are used to grow LSMO and LCMO films.

To study interfaces between $LaAlO_3$ and $SrTiO_3$, the growth should be controlled on the atomic scale and it is possible when the initial surface of the substrate is atomically smooth. To fabricate a single type interface, one layer of the initial substrate has to be terminated by either SrO or TiO_2. A thermal and chemical treatment is used to form perfectly crystalline TiO_2-terminated $SrTiO_3$ surfaces [2, 3]. Singly terminated TiO_2 surface shows unit cell step height (Figure 3.1d), the steps are clearly visible in Figure 3.1c. The single-terminated SrO surfaces can best be obtained by deposition of a SrO monolayer on a single terminated TiO_2 surface [4, 5]. In this thesis, only TiO_2-terminated surfaces are used and they were treated in TSST B.V, Enschede, the Netherlands.

Neodymium Gallate, $NdGaO_3$ offers less strain when compared to the $SrTiO_3$ substrate. The lattice parameters for the orthorhombic cell are a = 5.426 Å, b = 5.502 Å, c = 7.706 Å while for a perovskite-related cell a = b = 3.864 Å; c = 3.853Å, $\gamma_p = 89°$ [6]. Strontium Lanthanium Gallate ($SrLaGaO_4$) has a tetragonal structure with a = b = 3.843 Å and c = 12.68 Å and it is slightly compressive LSMO and LCMO films. Lanthanum Aluminate, $LaAlO_3$ offers compressive strain and can also be represented as pseudocubic with a = 3.793 Å. We will use the cubic indexing for LAO in this thesis (a_c = 3.79 Å).

Substrate/Thin films	LSMO 3.873 Å	LCMO 3.863 Å	LAO 3.79 Å
STO (3.905 Å)	-0.82%	-1.07%	-2%
NGO (3.851 Å)	0.6%	0.3%	x
LSGO (3.843 Å)	0.78%	0.52%	x
LAO (3.79 Å)	2.2%	1.9%	0%

Table 3.1: Strain between substrates and thin films with respect to the bulk lattice constants. The cross sign represents that this combination of film and substrates is not used in this thesis.

The nomenclature

It will be useful to define the nomenclature which we shall use in the rest of the thesis to refer to films and their respective substrates. The thin films of LSMO are indicated by LS, in brackets we shall put the thickness in nanometer, $LS(21)$ and the substrate is put in the subscript, $LS(21)_{STO}$. The thin films of LCMO are denoted with L and LAO as LA.

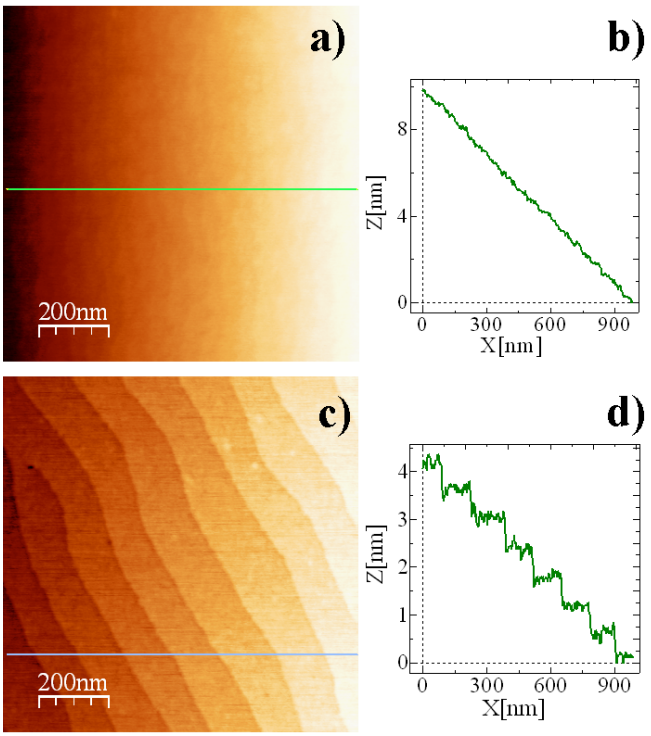

Figure 3.1: Surface analysis of STO substrate by atomic force microscopy (AFM). Untreated STO substrate is shown in (a) and it profile in (b). Parts (c) and (d) show a treated STO substrate. The profile (d) indicates the unit cell step height.

Thin film growth process

A schematic front view of the sputtering system is shown in Figure 3.2. A rotary feedthrough is connected to the center of the top flange, which can be lifted up by an electrical motor. A cross-piece with electrical and water feedthroughs, a plate with quartz crystal and heater element are connected to the rotary feedthrough. The substrate heater is surrounded by a cooling shroud to prevent the system and the temperature sensitive pressure gauges from temperature fluctuations. Four sputtering guns are mounted facing upward and the substrate heater can be rotated to be on on-axis with the each available cathode [7].

The substrate is glued on heater with a conducting silver paste. The silver paste remains conducting at high temperatures with melting point of 960°C. Four old STO samples are glued around the substrate to ensure the homogeneity of the temperature. The substrate and side plates are pre-baked at 300°C in air to make the glue harder in order to sustain high temperatures. A heater cover with a hole of 1.5 cm is used to have only substrates and side plate face the plasma, which helps to avoid contamination of the whole heater. The system is pumped down

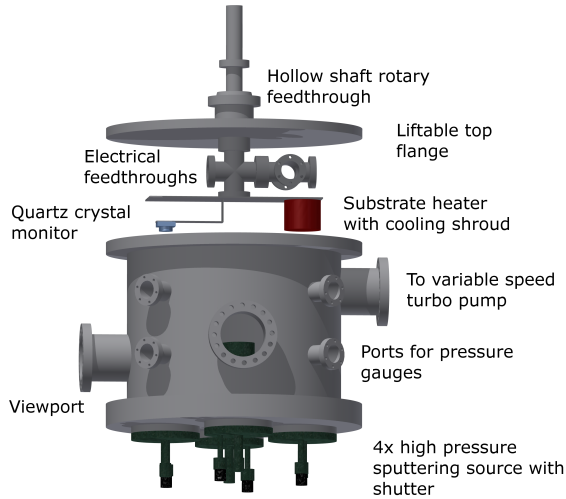

Figure 3.2: A 3d schematic view of the oxide sputtering system.

with a turbo pump for at least 8 hours which achieves a pressure of 1×10^{-6} mbar. Oxygen with purity of 99.999 % is entered into the system monitored by a flow meter. The pressure is regulated with the speed of the turbo pump, controlled by software. In DC sputtering, the targets are pre-sputtered at 1 mbar at a current of 100 mA and then deposition is done at a current of 350 mA at 3 mbar or 2.2 mbar. In RF sputtering, 20 W power is used for pre-sputtering and 30 W or higher power for deposition. The substrate holder which contains a heater is set to the optimized deposition temperature (which is 840°C for conducting films of LSMO and LCMO and 920°C for stoichiometric and non-stoichiometric LAO targets) and then the substrate holder is rotated on the top of plasma to deposit thin films of the required material. After deposition, the samples were cooled down in vacuum. Some samples of $LaAlO_3$ were cooled down in the growth pressure of oxygen but no significant changes were observed in properties of thin films.

3.2 Surface and structure characterization

Atomic force microscopy was used to view topography of all the LSMO, LCMO and LAO films. To investigate the quality of the films, we used x-rays diffraction.

3.2.1 Atomic Force Microscopy

All grown thin films are characterized by atomic force microscopy in tapping mode which provides better resolution of the images. AFM shows the quality of film surfaces in terms of flatness, roughness, and height profile. In tapping mode, the

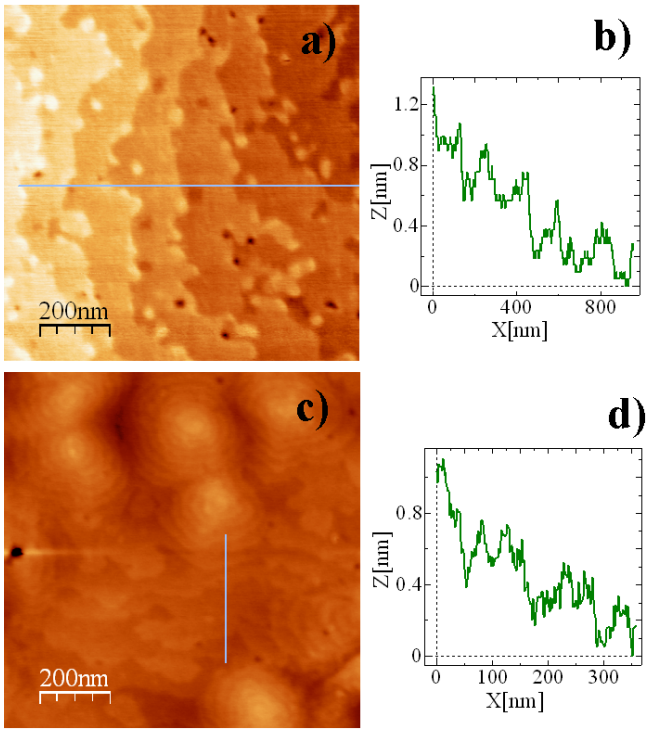

Figure 3.3: (a) Surface morphology of a 12 nm film of LSMO on STO, (b) the variation in height profile of (a) the step height is 0.4 nm. (c) A 35 nm film of LSMO on STO, shows spiral type morphology on some parts. The line profile (d) of the film is taken from the smoother part of the film. The overall roughness is 2 nm.

cantilever (driven by a piezoelectric actuator) vibrates at its resonance frequency. Upon approaching the sample, the tip briefly touches (taps) the surface at the bottom of each swing, resulting in a decrease in oscillation amplitude. The feedback loop keeps this decrease at a preset value and a topographic image of the sample surface can be obtained.

Figure 3.3 shows two films of LSMO on STO of thickness 12 nm and 35 nm. In Figure 3.3a, a very thin LSMO film shows the unit cell step height variation of the STO substrate. This indicates epitaxial match with the substrate. The thick film shown in Figure 3.3c shows spiral type morphology. At some portions, the steps can be seen. The roughness of 12 nm thick film is 0.4 nm while thick films are rougher because of more layers of material being deposited.

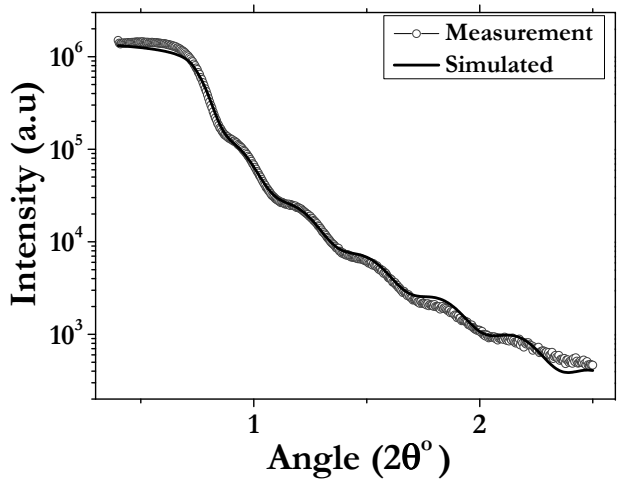

Figure 3.4: An X-ray reflectivity curve for a 24 nm thick film LCMO on STO (L598). The period of oscillation determines the thickness of film.

3.2.2 X-ray reflectometry (XRR)

X-ray reflectometry (XRR) is a non-contact, non-destructive analytical technique to determine thickness, density, and roughness of thin films. The basic idea behind the technique is to irradiate the sample with a beam of x-rays at very low angles. Increasing the angle of irradiation beyond a critical angle (depend on material), reflects the x-rays from interfaces and gives rise to interference fringes. The periodicity of the fringes is proportional to the thickness of the film. If the interface is not perfectly sharp and smooth then the reflected intensity will deviate from that predicted by the Fresnel law of reflectivity. This drop of intensity corresponds to the roughness of the films and the amplitude of the fringes is proportional to the density of the top and bottom layers. Figure 3.4 shows a film of 24 nm thick film of LCMO on STO. The number of fringes indicate the thickness and high intensity indicates the low interstitial roughness.

3.2.3 X-ray Diffraction (XRD)

X-ray diffraction is used to study the structure of thin films. We used a Siemens d500 diffractometer and a PAN analytical X-ray detector in Leiden to investigate the phase composition of thin films and the lattice constants. Figure 3.5 shows a typical way to measure lattice parameters. Taking STO as a reference, the lattice parameter of the film is calculated using Bragg's relation (d $\sin\theta$ = n λ). Figure 3.5 shows a 20 nm thin film of LSMO on STO. The mismatch between film and substrate is about -1.4%.

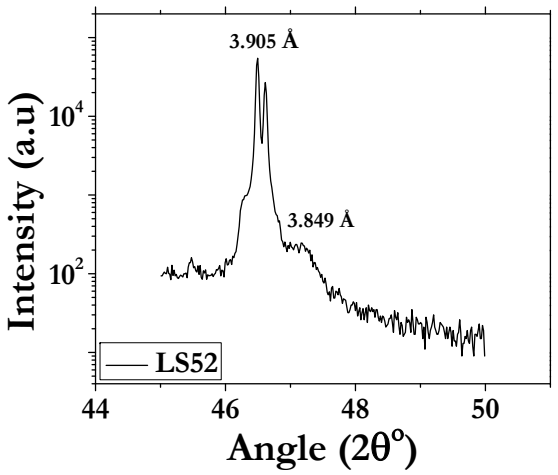

Figure 3.5: An XRD analysis of a 20 nm thin film of LSMO on STO.

3.2.4 Reciprocal Space Mapping (RSM)

High resolution XRD (RSM) measurements were performed with a Bruker D8 discoverer, equipped with a monochromator ($\lambda = 1.5406$ Å) and a Vantec-1 array detector in Twente University by Dr. S. Harkema. RSM measurements were performed on some films of LSMO, LCMO and LAO. The advantage of reciprocal space mapping is that the Bragg reflection under investigation is fully mapped in a confined area in Q-space. This means that the reflection is not only monitored by rocking curve crossing it but all directions are included in the measurement. This gives extra advantage to the non-symmetry of the crystals and to the epitaxy of the thin films. RSM maps for LCMO thin films are shown in section 3.5.

3.3 Lithographical techniques for pattering

We have used both optical and electron beam lithographic techniques to pattern LSMO and LCMO thin films to measure transport properties of these thin films. Figure 3.6 shows the basic process for optical and electron beam lithographic techniques. For positive resists, the resist is exposed with UV light or electron beam to remove the underlying material. The chemical structure of the resist becomes more soluble in the developer after exposure. The developer solution is washed away the exposed resist. Negative resists behave in just the opposite manner. Exposure to the UV light or electron beam causes the negative resist to become polymerized, and more difficult to dissolve. Therefore, the negative resist remains on the surface wherever it is exposed. The developer solution removes only the unexposed portions.

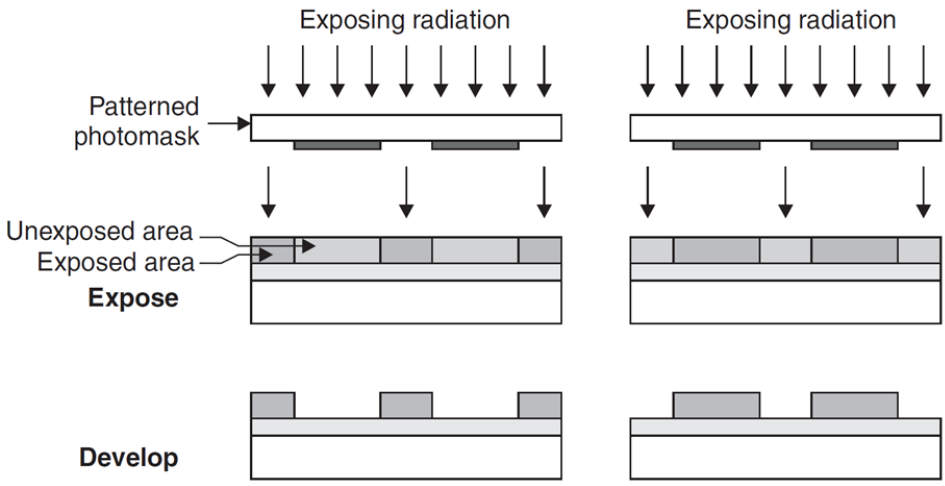

Figure 3.6: Lithographic operation with positive and negative resist (a) positive resist removes the exposed area and (b) negative resist leaves on the expose area after exposure and developing

3.3.1 Optical lithography

The LCMO and LSMO thin films were structured optically in a Hall bar geometry to investigate the effect of strain on carrier density. The structure is about 200 μm wide and the distance between the voltage contacts was 1.2 mm. A positive resist MaP1205 was spun on to the sample with 6000 revolution per minute (rpm). The sample was baked at 120°C for 120 seconds. After that sample was exposed to UV light for 15 sec. Then it was developed in MaD532 for 15 seconds. LSMO films were structured using wet etching (H_2O: 49% HF: HCl: HNO_3 = 25: 1: 1: 1) with an etch rate of 2 nm per minute for LSMO films. LCMO thin films were etched using argon ion etching with an etch rate of 0.3 nm/sec. After Ar-etching, the LCMO films were treated with an oxygen plasma in order to restore the insulating properties of the STO substrate [8].

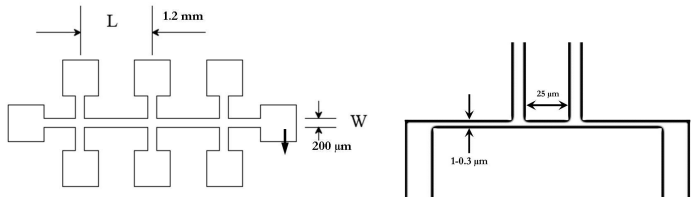

Figure 3.7: (Left) A standard Hall bar, (right) a structured patterned written with e-beam for small bridges, not to scale.

3.3.2 Electron beam lithography

We have used electron beam lithography to pattern small bridges for measuring the Hall effect and current-voltage characteristics. For this a Raith e-line machine was available which is a high resolution electron beam lithography system.

A Hall bar of width 50 μm (the distance between voltage contacts = 94 μm) was patterned on a few LCMO films. We also patterned thin films of LSMO and LCMO in small bridges of width from 1 μm down to 300 nm to measure current voltage characteristics, with a distance of 25 μm between voltage contacts.

A three step process was used to pattern Hall bar and small bridges. The typical structured patterns are shown in Figure 3.7. In the first step, Au markers were written because the contrast of LSMO or LCMO on STO is very poor. A lift-off process was used for this purpose: a bilayer of PMMA/MMA was spun on top of samples. The sample was baked at 180°C/120°C for 90/90 seconds and then only markers were written with e-beam. After developing, the sample was sputtered with gold in a Z400 sputtering system and then the lift off process is accomplished. In the second step, negative resist MaN2405 was spun onto the sample, and baked at 90° C for 10 minutes. Then the structure of LSMO or LCMO was written. After developing, the sample was etched either wet or by argon ion etching. In the third step, the first step was repeated but now for making Au contacts using the Au markers as reference.

3.4 Measuring properties of thin films

The transport properties of unstructured and structured thin films of LSMO and LCMO were measured using a physical properties measuring system (PPMS) from Quantum Design. The temperature range for the system is from 2 K to 400 K and magnetic field can be set up to 9 T. The temperature stabilization is better than 200 mK. External voltage and sources are used to measure structured and unstructured thin films, current-voltage behavior and Hall voltage. Different LabVIEW programs were designed to accomplish this task.

The magnetic properties of thin films were measured using a SQUID-based magnetic properties measuring (MPMS) from Quantum Design. The system can vary temperature between 2 K to 400 K and a magnetic field can be applied in transverse and longitudinal direction upto 7 T. We have measured Curie temperature T_c and the saturation magnetization to find out anomalous behavior in thin films of LSMO and LCMO.

3.5 Avoiding target degradation in sputtering manganite thin films

In this section, we address the issue of aging of the sputtering targets. After prolonged use (typically a few years), we find that the morphology of the films becomes poor: hole appear, step size become larger, and the roughness increases.

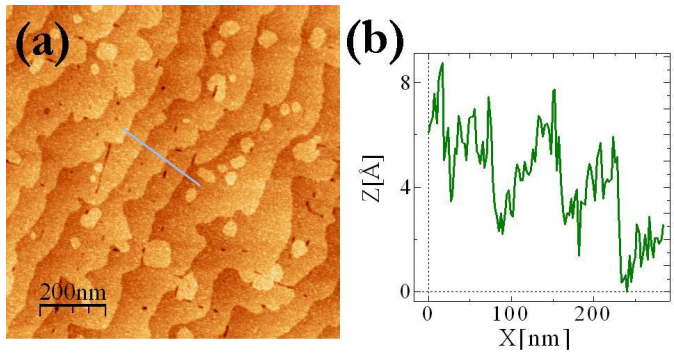

Figure 3.8: (a) Surface morphology of a 15 nm thin film of LCMO (L561) shows flat terraces. (b) The height profile gives step height of unit cell of 0.4 nm and the average roughness of the film is 0.2 nm.

We have performed experiments on the treatment of targets with water vapor in order to reverse their degradation. Below, we discuss the growth of films of LCMO on flat STO substrate before and after the target treatment.

3.5.1 Characteristic features of thin films of LCMO

Thin films of $La_{0.7}Ca_{0.3}MnO_3$ grown on $SrTiO_3$ substrate have characteristic features which can be distinguished by atomic force microscopy and transport properties. It is known that thin films of LCMO can be epitaxially grown on STO substrate, even though the mismatch (a_{LCMO} = 3.783 Å, a_{STO} = 3.905 Å, mismatch is -1%) leads to strained films. Still, they can be flat, with unit cell steps, which reflects the underlying substrate. In thick films, structural defects appear, the roughness also increases and steps are not visible anymore.

Figure 3.8a shows the topography of a 15 nm thin film of LCMO on STO grown with a new LCMO target. The film shows unit cell step height (Figure 3.8b). A detailed structural and interface analysis by HRTEM and EELS of these films is given elsewhere [9, 10].

Another distinguishing feature of LCMO thin films comes from the transport properties. Single crystal and very thick films of LCMO grown on any substrate show a T_{MI} of 270 K as shown in Figure 3.9 for a 75 nm film. In very thin films T_{MI} depends on lattice mismatch between substrate and film. STO produces tensile strain on LCMO whose in-plane lattice constant elongates Mn-O-Mn bond length and decreases Mn-O bond angle which suppresses the ferromagnetic state of LCMO, and reduces the transition temperature. It can be seen in Figure 3.9 that for a 11 nm film, T_{MI} is 130 K, 150 K less than the thicker one. A large reduction in resistance in LCMO films gives a large CMR effect [11] which is another characteristic feature of these films.

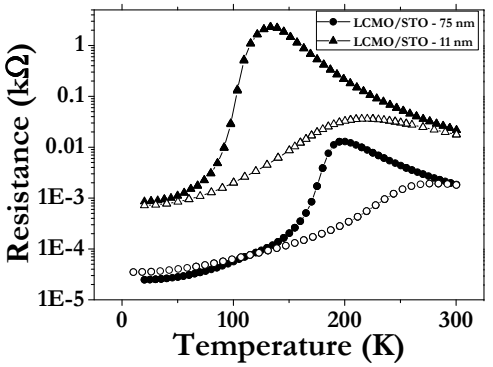

Figure 3.9: Temperature dependence of resistance for two films of LCMO on STO, a 75 nm film (shown in square symbols) and a 11 nm thin film (shown in triangles). Filled symbols represent the temperature versus resistance behavior at 0 T and open symbols at 9 T.

3.5.2 Observations-possible causes of rough films

We observed that thin films started to deteriorate with the passage of time without changing any growth parameters e.g., growth pressure, growth temperature, target to substrate distance, flow of oxygen. One of the films in this series of rough films is shown in Figure 3.10a. The growth time for this films is the same as shown in Figure 3.8a. It shows a structure of not well connected grains and holes as dark spots. The profile shows a non-homogeneous film which has a grain size of a 20 nm (Figure 3.10b). The rms surface roughness of this film is 5 nm.

The transport properties of such a film may show T_{MI} but also insulating behavior at low temperature as shown in Figure 3.11. Two thin films of 13 nm and 11 nm shown in Figure 3.11 and in Figure 3.9 respectively have approximately the same thickness but an insulating state shows up at low temperature for a film grown with an old target (L579). Some films grown with the old target show two or three resistance peaks (not shown here) which is improbable and indicates that films do not have the properties of LCMO films.

3.5.3 Hypothesis - role of Oxygen in LCMO

We see in the last two figures that thin films of LCMO are not good. They show large grains, are very rough and insulating. Without changing any growth parameters, the target was working for a long time to grow epitaxial LCMO films. We also observed a seasonal change in morphology which might be due to the humidity level which can effect the oxygen content in the growing films. We also know that the correct oxygen content is an important ingredient for high quality thin films of manganites. The role of oxygen stoichiometry is extensively studied for the colos-

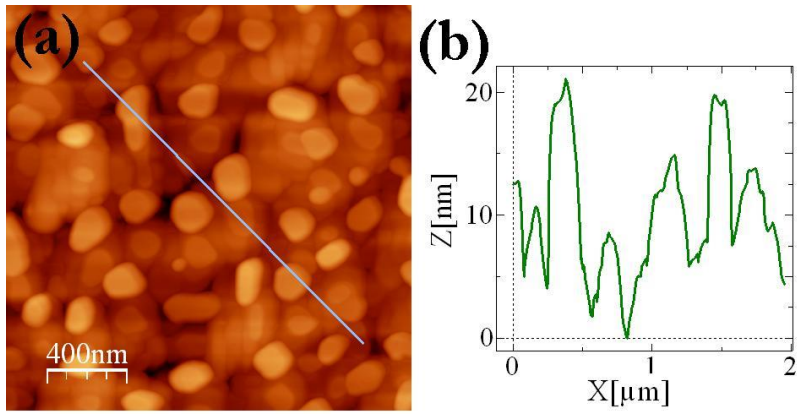

Figure 3.10: (a) Surface morphology of a 13 nm thin film of LCMO (L579) with a relatively old target (b) The height variation is 20 nm and rms roughness is 5 nm.

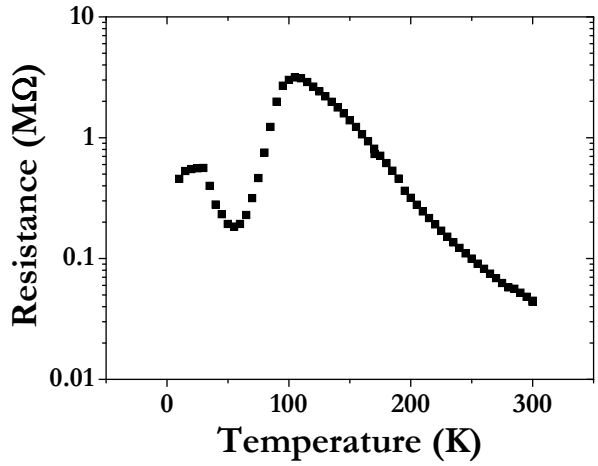

Figure 3.11: Temperature dependence of resistance of a 13 nm film of LCMO on STO (L579), the morphology of same films is shown in Figure 3.10.

sal magnetoresistive manganites [12–17]. The deficiency of oxygen can influence the crystalline structure, transport and magnetic properties of thin films [18, 19]. The preparation conditions are important for the growth of thin films and the oxygen content can be varied by changing the pressure of ambient gas or by post annealing [20]. The oxygen deficient films can be very rough and highly resistive.

Like manganites, high T_c superconductor YBCO has also been studied for the sensitivity of different growth parameters [21]. These critical growth parameters give a narrow window for epitaxial growth of thin films. Krupke *et al.* explained it as possible change in thin films of YBCO for a prolonged used target [22] and suggested treatment with water vapors [23]. Addition of water vapors produces atomic oxygen which triggers the film composition by increasing the atomic oxygen pressure since the dissociation of O_2 in a microwave discharge is almost entirely due to nitrogenous and hydrogenous impurities, as proved by Kaufmann and Kelso [24]. Costa *et al.* [25] and Brown *et al.* [26] showed that enhanced atomic oxygen content in the plasma was caused by a reduced combination rate of atomic oxygen at the chamber walls. In any case, each hydrogen atom introduced produces about 300 extra oxygen atoms which can be used to condition the old LCMO target. The poor morphology which shows holes in LCMO thin films may be caused by the LCMO target itself. The target might have exceeded its life time which results in reduced oxygen stoichiometry in the growing films.

3.5.4 Results-Reutilizing the LCMO target

Assuming the possible loss of oxygen in LCMO target, we treated the target with external oxygen in form of water vapors. A small reservoir of water was connected to the vacuum chamber which can be controlled by a power supply. The water pressure was optimized with respect to the base pressure of the system and few μbar of water vapors ware introduced in the system. The base pressure of our system is 1×10^{-6} mbar. The added water vapor is the water pressure at which thin films have been grown. The system was stabilized at water pressure for about one hour and then a specific process of pre-sputtering, sputtering and deposition was started. As this process relates to the dissociation of oxygen atoms, we name it pressure controlled oxygen dissociation (PCOD). The optimized water pressure in which high quality thin films are grown was 5×10^{-5} mbar. Below this pressure, films have holes and above this pressure, strange features in morphology were observed.

We have grown thin films at three different water pressures. Three pressures which show significant variation in morphology and structure are given in Table 3.2. We use three representative films to explain the growth of LCMO films at these water pressures.

Figure 3.12 shows three films grown at the water pressures given in Table 3.2. Film at pressure P1 is smooth but it shows some decorated outgrowth, following the steps of the substrate (Figure 3.12a). The step size is also higher than 2 nm. The film grown at P2, shown in Figure 3.12c, is very rough. The grainy structure is clearly seen. We have grown another film at a pressure in between theses two

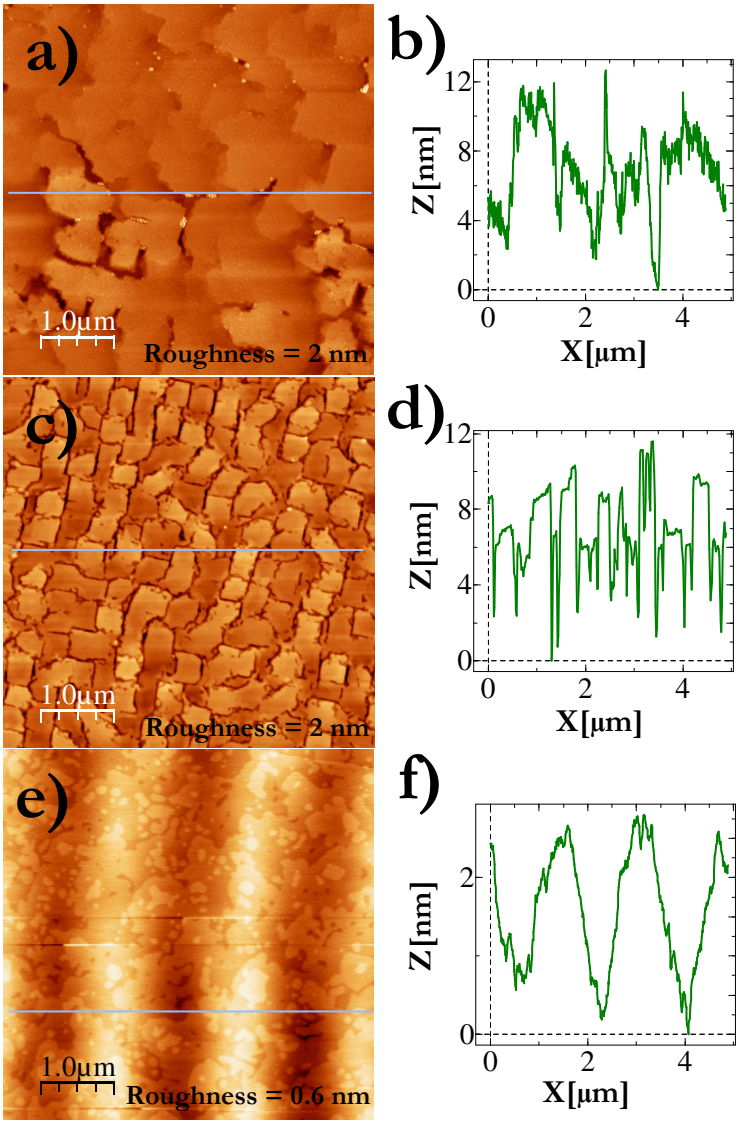

Figure 3.12: Effect of external oxygen on the morphology of thin films of LCMO. According to table 3.2 at pressure P1(L581) (a,b) at pressure P2 (L582)(c,d) at pressure P3 (L589) (e,f).

P_{water}(mbar)	Process ID	Roughness (nm)	d_{LCMO} (nm)	Sample ID
1×10^{-4} mbar	P1	2	x	L580
1×10^{-5} mbar	P2	2	10	L581
5×10^{-5} mbar	P3	0.6	24	L589

Table 3.2: Treatment of oxidized LCMO target at different water pressures to optimize the growth of thin films of LCMO. Given are the pressures used to optimize water content represented by P_{water} mbar, the process ID related to water-pressure, the roughness in nm, thickness of film d_{LCMO} (nm), and the relative sample identity ID.

pressures, P3. In Figure 3.12e, the film shows flat terraces with roughness of 0.2 nm.

The thickness of the films was measured by XRR. It is important to note that for film P1, fringes could not be found. We used XRD for structural analysis of the films. The diffraction plane (002) can only be found for the films grown by P3 while for the other films, no film peak can be seen.

LCMO thin films were analyzed by reciprocal space maps (RSM) which gave a good analysis of the epitaxy of the films. Figure 3.13 shows a reciprocal space map of the 10 nm film of LCMO on STO (L589) grown by P3 around the reflection (123). The peak of the film can be seen above the substrate peak (a very bright spot at the center). The out-of-plane lattice constant determined with this reflection is 0.382 nm. The in-plane peak values for film and substrate is the same, which shows that the film is epitaxial. The corresponding values of the in-plane lattice constant for film and substrate is 0.39 nm.

Figure 3.14 shows the resistance versus temperature behavior and it is clear that film grown at P3 has a transition temperature of 160 K as expected for this thickness (10 nm), while other three films do not have any transition which means that they do not have the properties correct LCMO. So, the optimized growth water pressure is P3, 5×10^{-5} mbar. At this pressure, we can grow high quality epitaxial manganite thin films of LCMO.

3.5.5 Pre-conditioning only

The purpose of water vapor addition to the sputter gas was to condition the target. We also tested film growth where we pre-sputter the target with water but closed its supply while depositing. The films grown in this way showed good morphology, crystallinity, phase and correct transition temperature corresponding to thickness of film. The only difference observed was that films which were grown with water have lower growth rate than done only by conditioning (pre-sputtering in water). This shows that the right tuning of water can compensate the deficiency of oxygen in old LCMO target.

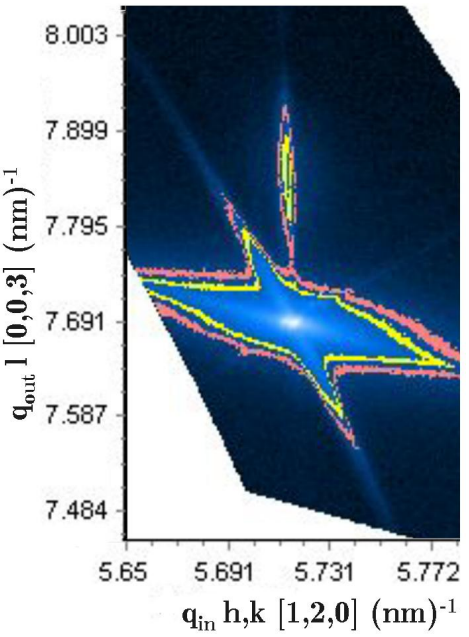

Figure 3.13: A reciprocal space map of 10 nm thick LCMO film on STO (L588) around the [123] reflection grown by P3. The film peak can be seen at 7.85 nm^{-1}.

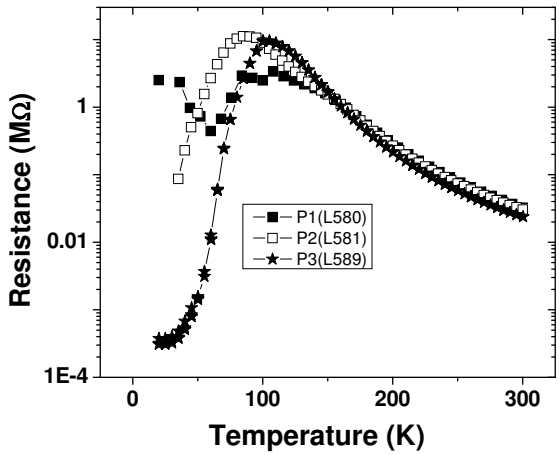

Figure 3.14: Transport properties of thin films of LCMO on STO (001) after treatment of target under different water pressures (see Table 3.2).

3.5.6 Role of substrate orientation

We described the effects of additional oxygen on thin films of LCMO on STO (001) substrates. This conditioning/treatement works also well for flat substrates of LSGO (001) and on NGO (001). The process does not work for substrates which have higher miscut angles or different orientation of planes, e.g., STO (110) and 1^o stepped STO (001). The different orientation of planes in theses substrates may require different water pressure to be optimized or a different growth temperature.

3.5.7 Conclusion

Thin films of LCMO were treated by water on flat STO (001) substrate using the PCOD process. Highly epitaxial thin films with the correct transition temperature depending on thickness on strained STO can be obtained in this process. The process also worked by only conditioning the target and stopping the water supply during growth, which increased the growth rate of thin films of LCMO. The optimized water pressure only worked for flat substrates with (100) orientation while stepped STO (001) and STO (110) may need to re-calibrate at a different water pressure.

Bibliography

[1] D.A. Glocker, S.I. Shah, Hand book of thin films process technology, Vol. **1**, IOP publishing Ltd, 2002.

[2] M. Kawasaki, K. Takahashi, T. Maeda, R. Tsuchiya , M. Shinohara, O. Ishiyama, T. Yonezawa, M. Yoshimoto and H. Koinuma, Science **266**, 1540 (1994)

[3] G. Koster, B.L. Kropman, G.J.H.M. Rijnders, D.H.A. Blank and H. Rogalla, Appl. Phys. Lett. **73**, 2920 (1998).

[4] S. Migita, Y. Kasai, S. Sakai, J. Low Temp. Phys. **105** , 1337 (1996).

[5] R. Takahashi, Y. Matsumoto, T. Ohsawa, M. Lippmaa, M. Kawasaki, and H. Koinuma, J. Cryst. Growth **234**, 505 (2002).

[6] S. Geller, Acta Cryst. **10**, 243 (1957).

[7] S. Freisem, PhD thesis, University Leiden, the Netherlands (1999).

[8] C. Beekman, I. Komissarov, M. Hesselberth and J. Aarts, Appl. Phys. Lett. **91**, 062101 (2007).

[9] J. Aarts, S. Freisem, R, Hendrix, H.W. Zandbergen, Appl. Phys. Lett. **72**, 2975 (1998).

[10] Z.Q. Yang, R. Hendrix, J. Aarts, Y.L. Qin, H.W. Zandbergen, Phys. Rev. B **70**, 174111 (2004).

[11] S. Jin, T.H. Thiel, M. McCormack, R.A. Fastnacht, R. Ramesh, and L.H. Chen, Science **264**, 413 (1994).

[12] C. Ritter, M.R. Ibarra, J.M.D. Teresa, P.A. Algarabel, C. Marquina, J. Blasco, J. Garcia, S. Oseroff, and S.-W. Cheong, Phys. Rev. B **56**, 8902 (1997).

[13] Z.L. Wang, J.S. Yin, Y.D. Jiang, and J. Zhang, Appl. Phys. Lett. **70**, 3362 (1997).

[14] J. Li, C.K. Ong, J.-M. Liu, Q. Huang, and S.J. Wang, Appl. Phys. Lett. **76**, 1051 (2000).

[15] R. Cauro, A. Gilabert, J.P. Contour, R. Lyonnet, M.-G. Medici, J.-C. Grenet, C. Leighton, and I.K. Schuller, Phys. Rev. B **63**, 174423 (2001).

[16] X.F. Song, G.J. Lian, and G.C. Xiong, Phys. Rev. B **71**, 214427 (2005).

[17] N. Malde, P.S.I.P.N. de Silva, A.K.M.A. Hossian, L.F. Cohen, K.A. Thomas, J.L. MacManus-Driscoll, N.D. Mathur, and M.G. Blamire, Solid State Commun. **105**, 643 (1998).

[18] S.J. Liu, J.Y. Juang, J.-Y. Lin, K.H. Wu, T.M. Uen, J. Appl. Phys. **103**, 023917 (2008).

[19] M. Rajeswari, R. Shreekala, A. Goyal, S.E. Lofland, S.M. Bhagat, Appl. Phys. Lett. **73**, 2672 (1998).

[20] A. Goyal, M. Rajeswari, R. Shreekala, S.E. Lofland, S.M. Bhagat, T. Boettcher, C. Kwon, R. Ramesh, and T. Venkatesan, Appl. Phys. Lett. **71**, 2535 (1997).

[21] J.R. Gavaler, J. Talvacchio, T.T. Braggins, M.G. Forrester, and J. Greggi, J. Appl. Phys. **70**, 4383 (1999).

[22] R. Krupke, Z. Barkay, G. Deutscher, Physica C **289**, 146 (1997).

[23] R. Krupke, Z. Barkay, G. Deutscher, Physica C **315**, 99 (1999).

[24] F. Kaufman, J.R. Kelso, J. Chem. Phys. **32**, 301 (1960).

[25] M.D. Costa, P.A. Zuliani, and J.M. Deckers, Can. J. Chem. **57**, 568 (1979).

[26] R.L. Brown, J. Chem. Phys. **71**, 2492 (1967).